

# A Stacked Analysis of Brightest Cluster Galaxies Observed with the *Fermi* Large Area Telescope

K. L. Dutson<sup>1\*</sup>, R. J. White<sup>1</sup>, A. C. Edge<sup>2</sup>, J. A. Hinton<sup>1</sup> and M. T. Hogan<sup>2</sup>

<sup>1</sup>*Department of Physics and Astronomy, The University of Leicester, University Road, Leicester, LE1 7RH, UK*

<sup>2</sup>*Department of Physics, Durham University, South Road, Durham, DH1 3LE, UK*

Accepted 2012 November 22. Received 2012 November 22; in original form 2012 September 14

## ABSTRACT

We present the results of a search for high-energy  $\gamma$ -ray emission from a large sample of galaxy clusters sharing the properties of three existing *Fermi*-LAT detections (in Perseus, Virgo and Abell 3392), namely a powerful radio source within their brightest cluster galaxy (BCG). From a parent, X-ray flux-limited sample of 863 clusters, we select 114 systems with a core-dominated BCG radio flux above 50/75 mJy (in the NVSS and SUMSS surveys, respectively), stacking data from the first 45 months of the *Fermi* mission in three energy bands, to determine statistical limits on the  $\gamma$ -ray fluxes of the ensemble of candidate sources.

For a  $>300$  MeV selection, the distribution of detection significance across the sample is consistent with that across control samples for significances  $<3\sigma$ , but has a tail extending to higher values, including three  $>4\sigma$  signals which are not associated with previously identified  $\gamma$ -ray emission. Modelling of the data in these fields results in the detection of four non-2FGL *Fermi* sources, though none of these appear to be *unambiguously* associated with the BCG candidate. Only one is sufficiently close to be a plausible counterpart (RXC J0132.6–0804), and the remaining three appear to be background AGN. A search at energies  $>3$  GeV hints at emission from the BCG in A 2055, which hosts a BL Lac object.

There is no evidence for a signal in the stacked data, and the upper limit derived on the  $\gamma$ -ray flux of an average radio-bright BCG in each band is at least an order-of-magnitude more constraining than that calculated for individual objects.  $F_{1\text{GeV}}/F_{1.4\text{GHz}}$  for an average BCG in the sample is  $<15$ , compared with  $\approx 120$  for NGC 1275 in Perseus, which might indicate a special case for those objects detected at high energies. The tentative suggestion that point-like *beamed* emission from member galaxies comprise the dominant bright  $\gamma$ -ray sources in clusters, implies searches for evidence of dark matter annihilation or large scale merger shock signatures for example, need to account for a significant level of contamination from within each cluster, that is both highly stochastic and varies significantly over time.

**Key words:** galaxies: active – galaxies: clusters: general – gamma rays: observations – radio continuum: general – radiation mechanisms: non-thermal – (galaxies:) cooling flows

## 1 INTRODUCTION

Feedback from the central active galactic nucleus (hereafter AGN) within a cooling-core cluster of galaxies is considered to play an integral large-scale role in the suppression of the observed cooling flow (see e.g. Fabian et al. 2002; Sijacki et al. 2007; Bower et al. 2006). The hot, diffuse, intracluster gas, which comprises 90% of the baryonic matter of the cluster and is bound gravitationally by a cold dark mat-

ter (DM) halo, is revealed observationally through thermal Bremsstrahlung emission in the X-ray band. From velocity dispersion measurements, the atmosphere of this intracluster medium (ICM) typically has a temperature between  $10^7$  and  $10^8$  K (McNamara & Nulsen 2007). The gas loses energy to radiation primarily in the X-ray band, condensing onto the central galaxy, and sub-sonic, pressure-driven inflows develop within the dense cooling region, where the radiative cooling time for such emission  $t_{\text{cool}}$ , is less than the age of the system (Fabian 1994).

\* E-mail: kate.dutson@leicester.ac.uk

However, as evidenced by spectroscopic data from

current-generation X-ray observatories *Chandra* and *XMM-Newton*, emission predicted by the standard cooling-flow model from expected quantities of cooling gas is not detected (Peterson et al. 2003). This soft X-ray deficit necessitates some reheating mechanism that acts to replenish the energy being radiated away, thus quenching the cooling flow. An attractive agent for this feedback is the central AGN, whose outbursts would not only resolve the dearth of X-ray luminosity, but also account for the measured truncation at the high-mass end of the galaxy luminosity function (Benson et al. 2003).

Support for this explanation is given by high-resolution observations of cavities in the X-ray halo of many systems (e.g. Fabian et al. 2000; McNamara et al. 2000), coincident with radio synchrotron emission associated with the activity of the central engine. The AGN in the brightest cluster galaxy (hereafter BCG) injects energy into the ICM in the form of bubbles containing relativistic particles, which displace the thermal gas. So-called ‘ghost cavities’ have also been found using *Chandra*, interpreted as relics of past AGN activity; bubbles that have previously detached from the radio lobes and risen buoyantly through the ICM, no longer bright at 1.4 GHz. They are now known to be filled with *low-frequency* radio synchrotron emission (e.g. Clarke et al. 2005; Wise et al. 2007). This evidence implicates AGN outbursts as intermittent phenomena; the power output averaged over time of the central engine able to balance the radiative cooling of the cluster core. For a review of AGN heating in clusters of galaxies, see McNamara & Nulsen (2007).

Both models of galaxy formation/clustering, and of feedback, and observations (including those aforementioned in the hard X-ray and radio bands), establish galaxy clusters as hosts to significant non-thermal particle populations (Völk & Atoyan 1999; Blasi et al. 2008). The remaining tracer of cosmic ray (CR) acceleration is  $\gamma$  radiation, and several emission scenarios predict BCGs to be sources of high-energy (HE) and very-high-energy (VHE) photons, with spectra dependent on the dominant energy content of the AGN jets; the nature of the seed particles they inject into the ICM, the strength of the local magnetic field, and the target density around the inflated bubbles (e.g. Hinton et al. 2007).

Ultra-relativistic particles may play an important role on several different scales in and around BCGs in cooling-core clusters, for example in AGN jets, mini-halos, and cluster-scale halos.  $\gamma$ -ray emission may arise in each via a number of dissimilar processes (e.g. Pfrommer & Enßlin 2004). Primary CR electrons accelerated in jets, or re-accelerated fossil CRs in mini-halos will produce inverse Compton (IC) emission. Inelastic proton-proton collisions of *hadronic* CRs on the target medium will lead to  $\pi^0$  decay emission and IC emission from secondary (or cascade) (e.g. Blasi & Colafrancesco 1999; Aharonian 2002) electrons. Most of these BCG-driven processes will produce GeV emission that is point-like for current detectors. However, it should be noted that – being massive and DM-dominated – clusters of galaxies are expected sources of *extended*  $\gamma$ -ray emission via DM annihilation (Ackermann et al. 2010a). Similarly, treating galaxy clusters as long-term reservoirs of CR hadrons, diffuse HE emission from  $\pi^0$  decay of particles accelerated (for example) in cluster-scale accretion shocks is theorised (e.g. Pfrommer & Enßlin 2004). The various emis-

sion scenarios produce different spectral, temporal and spatial signatures at GeV energies. The repository of HE data afforded by the *Fermi Gamma-ray Space Telescope* (hereafter *Fermi*) since its launch in 2008, is therefore an attractive resource when used in conjunction with multiwavelength data. Whilst a detection of extended cluster emission at GeV energies is yet to be made (Ackermann et al. 2010b), point-like emission from a number of BCGs is seen and there is considerable potential for improving our understanding of this class of objects using GeV data.

To date, excluding systems whose AGN jets are favourably aligned close to the observer’s line of sight so as to boost emission via relativistic beaming – associated with ‘BL Lac’ objects within the *unified model* of active galaxies (Antonucci 1993) – only two BCGs have been confirmed as emitters of HE  $\gamma$  rays. These are NGC 1275 and M 87 (Abdo et al. 2009a,b): the dominant member galaxies of the cooling-core clusters Perseus and Virgo, respectively. Both are known to host bright central radio sources associated with the active nucleus (see Vermeulen et al. (1994); Asada et al. (2006) and Biretta et al. (1991); Sparks et al. (1996)), and are also detected at very-high energies (Aleksić et al. 2012; Aharonian et al. 2006). The multiwavelength emission of AGN is characteristically variable, and indeed the  $\gamma$ -ray flux is found to vary on timescales down to days in the case of NGC 1275 (Brown & Adams 2011); similarly for M 87 (Abramowski et al. 2012). Light-crossing-time arguments thus restrict the physical size of the emitting region responsible for, at least a component of, the  $\gamma$ -ray emission.

These sources are HE laboratories for the class of BCGs, and motivate a search for further instances of  $\gamma$ -ray activity within it. The purpose of this work is to conduct such a search, using data from the Large Area Telescope (LAT) on board the *Fermi* satellite, accumulated thus far over the mission lifetime. To this end, we set out to imitate a deeper observation than is currently achievable in HE  $\gamma$  rays given the sensitivity of the *Fermi*-LAT, by constructing a sample of many potential sources within the BCG class, and stacking the output of individual analyses.

We defend our derivation of a suitable sample of candidate sources in §2, and the *Fermi*-LAT analysis procedure then carried out for each target is described in §3. The results are presented in §4, and discussed in §5. Conclusions of the work are then drawn in §6.

## 2 TARGET SELECTION

Considering NGC 1275 to be prototypical of  $\gamma$ -ray sources within the class of BCGs, our selection criteria were therefore designed to identify similar objects. The key requirements were the presence of a massive cluster of galaxies and evidence of non-thermal activity in the BCG. We constructed a sample of candidates drawn from five parent catalogues of X-ray flux-limited galaxy clusters: the Brightest 55 (B55) Sample (Edge et al. 1990), the ROSAT Bright Cluster Sample (BCS) (Ebeling et al. 1998), the extended ROSAT Bright Cluster Sample (eBCS) (Ebeling et al. 2000), the ROSAT-ESO Flux-Limited X-ray (REFLEX) Galaxy Cluster Survey Catalogue (Böhringer et al. 2004), and the Massive Cluster Survey (MACS) (Ebeling et al. 2001), encom-

passing objects from both the Southern and Northern hemispheres and including the brightest clusters from low Galactic latitudes. We include two clusters (RXC J1350.3+0940 and RXC J1832.5+6848) that meet the eBCS flux limit but were mis-identified as AGN when the sample was published, due to the presence of a bright radio source, and for comparison, two X-ray-luminous clusters that contain known AGN (4C+55.16 (Hlavacek-Larrondo et al. 2011), and E 1821+643 (Russell et al. 2010)) though the cluster emission falls just below the eBCS limit once the AGN contribution is taken into account.

From this sample of 863 unique clusters (accounting for the small overlap between these five samples), we selected the 151 systems in which the BCG is detected above 50 mJy in the NRAO VLA Sky Survey (NVSS) (Condon et al. 1998) or 75 mJy in the Sydney University Molonglo Sky Survey (SUMSS) (Mauch et al. 2003). We took care to remove systems where the radio emission is from a cluster member projected close to the BCG. Of this sample we have higher resolution radio imaging from the VLA or ATCA telescopes at 5 and/or 8 GHz for the majority (114 of 151), which can be used to identify those sources with a significant, flat spectrum core component (Hogan et al. prep).

We have optical spectra for 148 of the 151 BCGs recognised by our radio selection, and of these 64% (97 objects), exhibit optical line emission. This is significantly higher than the 25–30% of BCGs in an X-ray selected sample presenting line emission, indicating that our radio selection strongly prefers clusters with a cooling flow (Burns 1990; Cavagnolo et al. 2008; Mittal et al. 2009; Hogan et al. prep).

The sample represents a complete selection of radio-bright clusters that is dominated by cooling-core clusters, spanning a wide range in redshift ( $0.009 < z < 0.45$ ). It can be divided into BCGs whose radio emission has some contribution from the core or is core-dominated, and those with extended radio morphology and a lobe-dominated radio flux. The former comprise 114 objects and constitute the ‘main sample’ (see Figure 1 and Table 1), with the remaining 37 BCGs forming an ‘extended sample’. We compiled a counter sample of 65 ‘control’ clusters drawn from the parent X-ray sample that do *not* contain a radio-bright BCG, nor optical emission lines, but share the same redshift distribution as the radio bright sample for a representative comparison. We also generated a pair of control samples of 114 candidate sources each with random positions on the sky (generated by performing first a positive and then a negative  $5^\circ$  shift in Galactic latitude on the coordinates of the main sample candidates) for direct comparison with the main sample.

The parent clusters of the main sample BCGs include hosts to five BL Lac objects, two of which are known HE  $\gamma$ -ray sources listed in the *Fermi*-LAT Second Source Catalog (2FGL) (Nolan et al. 2012): 2FGL J0627.1–3528 in A 3392 and 2FGL J1958.4–3012 in RXC J1958.2–3011. The other three BL Lacs, RGB J1144+676 in A 1366, RGB J1518+062 in A 2055 and B2 2334+23 in A 2627, are not known *Fermi* sources. These BL Lacs are included as the original cluster identification from the ROSAT Survey incorrectly attributed the (bulk of the) X-ray emission to the cluster (e.g. RXC J1958.2–3011, Böhringer et al. 2004). However, in all five cases, pointed *Chandra* or *XMM-Newton* observations indicate that the BL Lac dominates the emission, so the

cluster does not meet the X-ray flux limit applied to select the other clusters. Therefore even this small *Fermi*-LAT detection fraction is an upper limit, given only NGC 1275 (a misaligned blazar) and M 87 (a radio galaxy) are dominated by the extended X-ray emission from their host cluster, and hence meet the cluster selection criteria. For the purpose of the analyses detailed hereafter, these two well-studied BCGs are not included in the sample, since our aim is to identify whether any additional sources in the class are detected using *Fermi*. There is no *clear* cluster around RXC J1958.2–3011, so its classification as a BCG is not certain, but with this caveat in mind it is kept, particularly as an additional *Fermi* source to check the output of analyses against.

### 3 *Fermi*-LAT OBSERVATIONS AND DATA ANALYSIS

The *Fermi*-LAT is a pair conversion instrument sensitive to photons of energy  $\sim 20$  MeV –  $>300$  GeV, with a wide field of view (2.4 sr) and large effective area ( $\approx 8000$  cm<sup>2</sup> on axis at 1 GeV). The detector is described in detail in Atwood et al. (2009) and references therein. *Fermi* observations are taken primarily in *all-sky-survey* mode, in which the spacecraft is pointed at some angle from the zenith, and rocked north and south of its orbital plane, scanning the whole sky every  $\sim 3$  hours.

The 151 BCGs of our main and extended samples were treated as candidate point sources of HE  $\gamma$  rays, and each analysed using the *Fermi* Science Tools version v9r27p1, and instrument response function (IRF) P7SOURCE\_V6. Event and spacecraft *all-sky-survey* data amassed between the 4<sup>th</sup> of August 2008 and the 28<sup>th</sup> of April 2012 (a Mission-Elapsed-Time interval of 239557417 to 357308125, equating to  $\sim 1362$  days) were extracted for a source region (SR) of  $12^\circ$ , centred on each BCG position (taken from optical data in the literature) and in the energy range  $300 \text{ MeV} \leq E \leq 300 \text{ GeV}$  (thus discarding events at the lowest energies, where the high point spread function (PSF) results in considerable source confusion). A zenith cut of  $100^\circ$  was applied to eliminate  $\gamma$  rays from the Earth’s limb, and all ‘Source’ class events were considered.

For each candidate source the data were fitted to a source model constructed to describe (in addition to potential emission from the target BCG), the emission from nearby (i.e. within the SR) 2FGL sources, and the diffuse Galactic and extragalactic (isotropic)  $\gamma$ -ray backgrounds (thus recent models gal\_2yearp7v6\_v0.fits and iso\_p7v6source.txt respectively<sup>1</sup> were utilised; their normalisation free to vary). The photon index and normalisation for objects within  $1^\circ$  of the candidate position were allowed to vary. Outside of this region but within the specified *region of interest* (ROI) of  $8^\circ$ , the normalisation was free to vary, but the photon index was fixed to the 2FGL value. Sources outside of the ROI but within the SR were included in the model, but their aforementioned parameters were fixed to the catalogue values. In the event that a candidate position coincided with a 2FGL source (within  $0.2^\circ$ ), then that source

<sup>1</sup> <http://fermi.gsfc.nasa.gov/ssc/data/access/lat/BackgroundModels.html>

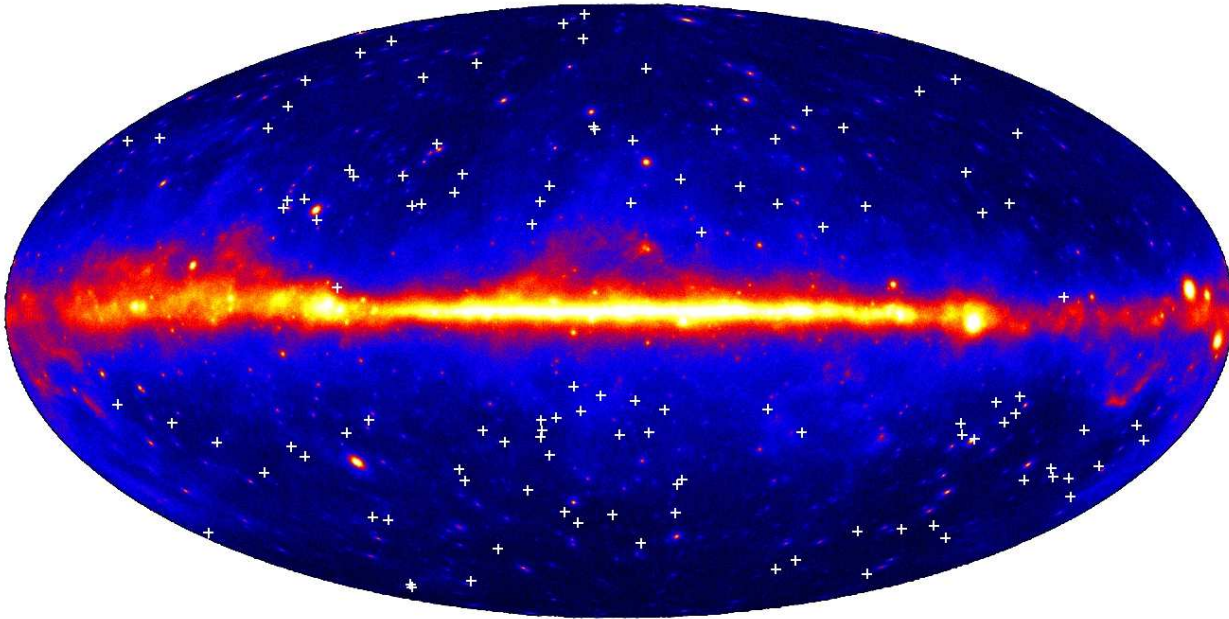


**Figure 1.** An all-sky map constructed from  $\sim 45$  months of  $300 \text{ MeV} \leq E \leq 300 \text{ GeV}$  *Fermi* data, scaled logarithmically. The BCG positions of the 114 candidates of the main sample are indicated by the white crosses.

was automatically removed from the model. This action provides a useful check of the output of our analyses against the catalogue values for known *Fermi* sources, whilst allowing all BCGs in the sample to be treated in the same way.

The maximum-likelihood spectral estimator *GTLIKE* was used to perform a *binned* fit, modelling the candidate source emission with a power law spectrum. *GTMODEL* was then used to obtain a model map of each candidate region given the result of the fit. To construct counts maps from the data *GTBIN* was utilised. Binned exposure cubes were also generated (through use of the *GTEXPCUBE2* tool) as part of the binned likelihood analysis chain. A binned method of likelihood fitting was adopted over an unbinned one, because it was found to be more robust, the fit converging irrespective of how many 2FGL sources a given SR contained.

The distribution of Test Statistic (TS) values (output by *GTLIKE*) across the sample could then be studied. A critical TS of 25 (corresponding roughly to a detection significance of  $5\sigma$  (Mattox et al. 1996)) was decided upon, below which an upper limit on the source emission was automatically calculated. All candidate sources with  $\text{TS} \gtrsim 16$  were nevertheless investigated on an individual basis: TS maps were constructed and any peaks found thereon fitted with parabolic ellipsoids to localise the emission. Where appropriate the data were then remodelled to constrain potential new *offset* sources.

The ensemble of counts maps constructed from the sample data, and that of the model maps output from fitting based on a *null* hypothesis (that is, the absence of a candidate *Fermi* source at the position of the BCG), were stacked. These stacked maps could then be sliced to provide 1-D comparisons between the summed model fit and the data. To derive an upper limit on the  $\gamma$ -ray flux of an average source in our sample using this stacking method, the stacked counts map was used to obtain a number of *on-source* counts ( $N_{\text{on}}$ )

within a region of radius comparable with the PSF of the LAT instrument on average across the selected energy band. An estimate of the number of background photons in this region,  $\hat{N}_{\text{B}}$  was obtained by similarly integrating the stacked model map. The number of *off-source* counts ( $N_{\text{off}}$ ) is then  $\hat{N}_{\text{B}}/\alpha$  where *alpha* is taken as the ratio of the solid angle in the chosen radius to that of the field of view. Thus an estimate of the  $\gamma$ -ray signal present is given by the excess counts,  $N_{\text{on}} - \alpha \cdot N_{\text{off}}$ . A 95% confidence upper limit on the signal was computed following the method of Rolke et al. (2005), assuming only Poisson errors on the background estimate. Whilst a more sophisticated likelihood method similar to that used by Huber et al. (2012) may provide a modest sensitivity improvement, our approach is simple and robust.

Weighted exposure maps were constructed for each candidate source and stacked, to provide a summed exposure map from which the exposure averaged over solid angle in the on-region could be determined. This value was used to transform our signal upper limit to an upper limit on the  $\gamma$ -ray flux. The rms variation in exposure across the sample is  $\approx 6\%$ .

For the purpose of investigating potential weak, hard spectrum, candidate source emission; less contaminated by the diffuse background, and given that stacking is most promising in the signal-limited regime, where every additional field adds potential source photons with minimal cost in background contamination, energy cuts above 3 GeV and 30 GeV were applied to the data and the analyses repeated in an otherwise identical manner; upper limits calculated within regions of radii comparable to the LAT PSF at the respective lower energy bounds. Corresponding analyses were performed simultaneously for the control and radio-quiet samples.

#### 4 RESULTS

A summary of the source properties of the BCGs of the main sample; their respective TS values and/or upper limits output from the analysis procedure outlined in §3 is given in Table 1. For the sake of clarity, the test statistic is shown as zero for sources with  $TS < 1$ . An upper limit is included for sources with  $TS < 25$ . Those BCGs with  $TS > 25$  are in:

A 3392

RXC J1958.2–3011

MACS J1347.5–1145

As noted in §2, the sources in A 3392 and RXC J1958.2–3011 correspond to the known *Fermi* sources 2FGL J0627.1–3528 and 2FGL J1958.4–3012, respectively. The BCG in MACS J1347.5–1145 is *not* in the 2FGL catalogue. These sources, and those that fall shy of the TS cut, but for which TS is greater than  $\approx 16$  are discussed in §4.3 below.

Table 1: A summary of the 114 brightest cluster galaxies of the main sample, and their candidate *Fermi* source properties, including the upper limit on the  $\gamma$ -ray flux above 300 MeV. The radio emission is classified as core-dominated ('c'), extended-with-core-contribution ('e') or BL Lac-associated ('b').

Parent Cluster	$l^*$ ( $^\circ$ )	$b^\dagger$ ( $^\circ$ )	$z$	1.4 GHz $^\ddagger$ Radio Flux (mJy)	TS $^\ddagger$	$\gamma$ -ray Flux Upper Limit (ph cm $^{-2}$ s $^{-1}$ )
RXCJ0000.1+0816	101.9	-52.5	0.04	84 c	0	$2.2 \cdot 10^{-10}$
A85	115.3	-72.0	0.056	58 c	0	$2.8 \cdot 10^{-10}$
Z235	120.8	-38.4	0.083	50 c	3.2	$5.7 \cdot 10^{-10}$
3C31	126.9	-30.3	0.016	1108 e	2.2	$5.8 \cdot 10^{-10}$
RXCJ0132.6-0804	152.0	-68.6	0.15	308 c	24.0	$1.6 \cdot 10^{-9}$
MACSJ0242.5-2132	206.6	-64.1	0.31	1255 c	0	$1.9 \cdot 10^{-10}$
A3112	253.0	-56.1	0.075	1915 c	11.2	$8.2 \cdot 10^{-10}$
A496	209.7	-36.5	0.033	121 c	5.8	$9.2 \cdot 10^{-10}$
RXCJ0439.0+0520	191.4	-26.2	0.21	82 c	6.0	$8.2 \cdot 10^{-10}$
NGC1650	214.0	-34.9	0.036	91 c	0	$5.0 \cdot 10^{-10}$
S555	243.6	-26.3	0.044	319 c	0	$2.1 \cdot 10^{-10}$
A3378	241.9	-24.0	0.14	1337 c	0	$2.9 \cdot 10^{-10}$
A3392	243.5	-20.0	0.055	4513 b	221.0	–
PKS0745-191	236.5	3.0	0.1	2373 c	13.7	$8.2 \cdot 10^{-10}$
A646	172.7	34.6	0.13	54 c	0	$8.3 \cdot 10^{-11}$
4C+55.16	162.3	36.6	0.24	8284 c	1.6	$4.9 \cdot 10^{-10}$
Hydra-A	243.0	25.1	0.054	40850 c	2.7	$4.8 \cdot 10^{-10}$
MACSJ1133.2+5008	150.7	62.6	0.39	846 e	0	$2.3 \cdot 10^{-10}$
A1348	277.4	47.1	0.12	158 c	0	$1.4 \cdot 10^{-10}$
A1366	132.6	48.5	0.12	237 b	0	$3.0 \cdot 10^{-10}$
NGC4696	302.5	21.6	0.0098	5674 e	0	$3.4 \cdot 10^{-10}$
MACSJ1347.5-1145	324.1	48.8	0.45	48 c	43.4	–
A1795	33.9	77.2	0.062	925 e	0	$1.9 \cdot 10^{-10}$
RXCJ1350.3+0940	344.3	67.7	0.13	293 c	0	$1.0 \cdot 10^{-10}$
A3581	323.2	32.9	0.023	646 c	7.4	$1.1 \cdot 10^{-9}$
A1885	83.2	66.6	0.089	49 c	0	$1.2 \cdot 10^{-10}$
S780	341.0	35.1	0.24	106 c	1.5	$3.1 \cdot 10^{-10}$
RXCJ1504.1-0248	355.1	46.2	0.22	62 c	7.3	$9.6 \cdot 10^{-10}$
A2052	9.5	50.1	0.035	5500 c	0	$2.4 \cdot 10^{-10}$
A2055	8.9	49.3	0.1	498 b	8.0	$8.4 \cdot 10^{-10}$
RXCJ1524.2-3154	337.1	20.7	0.1	50 c	2.0	$5.3 \cdot 10^{-10}$
RXCJ1558.3-1410	356.6	28.7	0.097	461 c	1.7	$6.8 \cdot 10^{-10}$
A2199	63.0	43.7	0.03	3681 e	1.5	$5.9 \cdot 10^{-10}$
NGC6338	85.9	35.4	0.028	57 c	0	$3.5 \cdot 10^{-10}$
Z8193	67.6	34.7	0.18	134 c	0	$2.7 \cdot 10^{-10}$
A2270	83.1	33.8	0.24	144 c	2.6	$5.1 \cdot 10^{-10}$
Z8276	58.0	27.6	0.076	92 c	0	$5.6 \cdot 10^{-10}$
RXCJ1750.2+3504	60.6	27.0	0.17	69 c	0	$1.5 \cdot 10^{-10}$
E1821+643	94.1	27.4	0.3	94 e	1.3	$2.7 \cdot 10^{-10}$
RXCJ1832.5+6848	99.2	26.8	0.2	150 c	0	$1.1 \cdot 10^{-10}$
A3639	347.0	-26.3	0.15	139 c	0	$2.1 \cdot 10^{-10}$
RXCJ1931.6-3354	5.2	-22.5	0.097	886 c	0	$2.8 \cdot 10^{-10}$
MACSJ1931.6-2634	12.6	-20.1	0.35	223 c	7.4	$1.0 \cdot 10^{-9}$
RXCJ1958.2-3011	11.0	-26.8	0.12	128 b	46.3	–
Cyg-A	76.3	5.8	0.056	1590000 e	4.5	$7.9 \cdot 10^{-10}$
S851	351.0	-32.6	0.0097	139 c	0	$9.3 \cdot 10^{-10}$
RXCJ2014.8-2430	18.4	-28.5	0.16	230 e	0	$3.4 \cdot 10^{-10}$
A2390	74.0	-27.8	0.23	236 c	11.2	$4.3 \cdot 10^{-10}$
RXCJ2213.1-2754	22.3	-55.0	0.061	76 c	0	$2.8 \cdot 10^{-10}$
A3880	18.1	-58.5	0.058	228 c	4.0	$5.7 \cdot 10^{-10}$
A2597	65.4	-64.9	0.085	1875 e	0	$1.9 \cdot 10^{-10}$
A2627	101.8	-35.9	0.13	434 b	9.8	$8.3 \cdot 10^{-10}$
A2634	103.6	-33.1	0.03	1037 e	0	$1.9 \cdot 10^{-10}$
RXCJ0137.2-0911	156.3	-69.1	0.041	178 e	0	$3.1 \cdot 10^{-10}$

Table 1 – *continued*

Parent Cluster	$l^\circ$	$b^\dagger(\circ)$	$z$	1.4 GHz <sup>‡</sup> Radio Flux (mJy)	TS <sup>††</sup>	$\gamma$ -ray Flux Upper Limit ( $\text{ph cm}^{-2} \text{s}^{-1}$ )
A262	136.6	-25.1	0.017	67 e	0	$4.3 \cdot 10^{-10}$
A2984	256.6	-68.9	0.1	232 c	0	$1.5 \cdot 10^{-10}$
A3017	256.6	-65.7	0.22	127 c	3.3	$5.1 \cdot 10^{-10}$
Z808	175.4	-47.3	0.17	393 e	0	$9.6 \cdot 10^{-11}$
A407	150.7	-19.9	0.048	661 c	0	$1.7 \cdot 10^{-10}$
RXCJ0331.1-2100	212.3	-53.2	0.19	168 c	0	$2.5 \cdot 10^{-10}$
NGC1399	236.8	-53.6	0.0051	2500 e	2.9	$4.8 \cdot 10^{-10}$
A3165	226.4	-51.4	0.14	921 c	0	$1.4 \cdot 10^{-10}$
RXCJ0359.1-0319	193.4	-39.3	0.12	188 e	0	$2.8 \cdot 10^{-10}$
RXCJ0425.8-0833	203.4	-36.2	0.04	112 e	0	$2.5 \cdot 10^{-10}$
MACSJ0429.6-0253	197.9	-32.6	0.4	139 c	0	$1.3 \cdot 10^{-10}$
A499	218.5	-38.3	0.15	158 e	0	$4.8 \cdot 10^{-10}$
RXCJ0501.4+0110	198.5	-23.7	0.12	121 c	0	$3.2 \cdot 10^{-10}$
MACSJ0520.7-1328	215.3	-26.1	0.34	93 c	0	$2.8 \cdot 10^{-10}$
A3360**	249.4	-30.7	0.085	222 c	0	$2.2 \cdot 10^{-10}$
S547	254.2	-30.0	0.051	143 e	0	$3.1 \cdot 10^{-10}$
A3380	257.2	-27.3	0.055	1455 e	1.0	$5.1 \cdot 10^{-10}$
A3396	250.0	-21.6	0.18	614 e	2.5	$2.4 \cdot 10^{-10}$
A795	217.1	40.2	0.14	116 c	1.1	$1.8 \cdot 10^{-10}$
S617	253.3	23.3	0.034	105 e	7.3	$7.5 \cdot 10^{-10}$
A907	249.4	33.3	0.17	69 c	0	$1.5 \cdot 10^{-10}$
A923	205.3	53.3	0.12	73 c	0	$1.9 \cdot 10^{-10}$
Z3179	228.7	53.1	0.14	94 c	6.6	$7.4 \cdot 10^{-10}$
Z3916	144.7	54.4	0.21	66 c	0	$9.0 \cdot 10^{-11}$
A1361	153.4	66.6	0.12	864 e	0	$3.0 \cdot 10^{-10}$
A3490	287.8	26.5	0.07	368 e	0	$2.0 \cdot 10^{-10}$
A1412	128.4	43.1	0.083	73 e	0	$2.0 \cdot 10^{-10}$
MACSJ1206.2-0847	284.5	52.4	0.44	161 e	0	$1.1 \cdot 10^{-10}$
A1644	305.0	45.4	0.047	98 c	0	$5.8 \cdot 10^{-10}$
A1677	84.0	85.1	0.18	76 c	0	$1.7 \cdot 10^{-10}$
NGC5098	78.8	81.3	0.036	83 c	0	$3.7 \cdot 10^{-10}$
A3565	313.6	28.0	0.012	3000 e	0	$5.4 \cdot 10^{-10}$
MACSJ1411.3+5212	97.6	60.8	0.46	22720 e	0	$3.9 \cdot 10^{-10}$
A2204	21.2	33.2	0.15	70 c	0	$1.3 \cdot 10^{-10}$
HerA	23.1	28.9	0.15	34000 e	3.6	$3.3 \cdot 10^{-10}$
NGC6269	49.1	35.9	0.035	51 c	3.0	$2.5 \cdot 10^{-10}$
RXCJ1715.1+0309	24.5	22.8	0.13	165 c	0	$2.7 \cdot 10^{-10}$
RXCJ1720.1+2637	49.3	30.9	0.16	89 e	0	$1.4 \cdot 10^{-10}$
RXCJ1840.6-7709	317.3	-25.8	0.019	1152 e	0	$2.3 \cdot 10^{-10}$
RXCJ1852.1+5711	87.1	22.4	0.11	51 c	0	$4.5 \cdot 10^{-10}$
A2312	99.0	24.8	0.095	79 c	5.4	$6.3 \cdot 10^{-10}$
A3638	355.4	-24.0	0.077	258 c	0	$2.4 \cdot 10^{-10}$
IC4991	359.9	-33.2	0.019	109 c	16.0	$1.6 \cdot 10^{-9}$
S868	22.9	-29.1	0.056	229 c	0	$2.1 \cdot 10^{-10}$
RXCJ2034.9-2143	23.2	-32.0	0.19	82 c	0	$3.4 \cdot 10^{-10}$
RXCJ2043.2-2144	23.9	-33.8	0.2	295 e	0	$1.8 \cdot 10^{-10}$
A2331	40.9	-31.7	0.079	106 e	5.3	$3.5 \cdot 10^{-10}$
RXCJ2101.5-1317	35.4	-34.8	0.028	1200 e	0	$1.9 \cdot 10^{-10}$
RBS1712	22.2	-38.8	0.19	67 c	0	$1.9 \cdot 10^{-10}$
APM699	338.1	-45.7	0.082	152 e	11.7	$9.8 \cdot 10^{-10}$
RXCJ2151.3-5521	339.2	-47.1	0.038	108 e	9.3	$3.0 \cdot 10^{-10}$
A2384	33.4	-48.4	0.096	54 c	0	$3.1 \cdot 10^{-10}$
A2389	53.7	-41.8	0.15	78 c	0	$3.6 \cdot 10^{-10}$
A2415	54.0	-45.1	0.058	187 c	0	$1.4 \cdot 10^{-10}$
A3856	2.8	-56.2	0.14	186 e	0	$1.6 \cdot 10^{-10}$
A2445	83.0	-30.8	0.17	77 c	6.0	$4.3 \cdot 10^{-10}$
A3911	336.7	-55.4	0.097	418 e	0	$1.5 \cdot 10^{-10}$

Table 1 – <i>continued</i>						
Parent Cluster	$l^*$ (°)	$b^\dagger$ (°)	$z$	1.4 GHz <sup>‡</sup> Radio Flux (mJy)	TS <sup>††</sup>	$\gamma$ -ray Flux Upper Limit ( $\text{ph cm}^{-2} \text{s}^{-1}$ )
S1101	348.4	-64.8	0.056	<i>472 c</i>	0	$3.0 \cdot 10^{-10}$
A4023	304.7	-31.7	0.19	<i>143 e</i>	0	$2.9 \cdot 10^{-10}$
A2665	97.0	-53.6	0.057	56 c	0	$1.7 \cdot 10^{-10}$

\* Galactic longitude

† Galactic latitude

‡ Taken from the NVSS. If italicised, the values instead denote the 843 MHz radio flux taken from the SUMSS

†† Test Statistic – for clarity TS values &lt;1 are shown as zero

\*\* Despite a low TS, this source was not included in the stacked analysis (see §4.2) due to the proximity of a bright 2FGL source, as detailed in the text



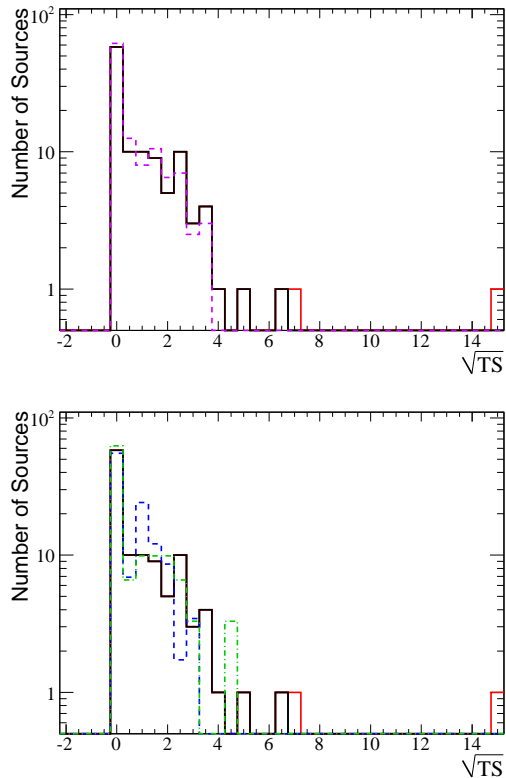


**Figure 2.** Histograms showing the comparison between the distribution of detection significance across the samples described in §2. The main sample of BCGs (black line) is included on both plots. **Top Panel:** The (averaged) control sample of random positions on the sky (dashed violet line). **Bottom Panel:** The scaled extended cluster sample (dot-dashed green line) and radio-quiet cluster sample (dashed blue line). The (two) sample BCGs with existing *Fermi* detections have been added in red.

#### 4.1 Distribution of Detection Significance

The distribution of  $\sqrt{\text{TS}}$  (corresponding approximately to the statistical significance, see §3) for each sample analysed is shown in Figure 2. The extended and radio-quiet cluster samples have been scaled appropriately, and the control samples averaged, so that comparisons may easily be made with the main sample of 114 objects. Common to all distributions is a clear peak at 0, and also a tail containing several signals at up to  $\approx 3\sigma$ . However this tail is more pronounced for the main sample – implying that a stacking analysis may be worthwhile (see §4.2 below) – and outliers are present: the high-TS sources are visible above  $4\sigma$  (see §4.3 below), including the two *Fermi* sources shown in red; all members of the main sample. The only exception is the extended sample BCG in S 753, for which a TS of 19.9 was derived. Inspection of the field containing this object reveals a highly confused region of diffuse emission, likely associated with the Galactic background, and as such this result is not believed.

#### 4.2 Stacking Analysis

The stacked analyses of the main sample above the three energy cuts – described in §3 – are illustrated in Figure 3. In each case the left panel shows the stacked counts map

in the colour scale, overlaid with contours defining the corresponding stacked model map for the null hypothesis. The maps to be summed were each centred on the candidate source position (0,0), which is marked on the final stacked plot. The right panels show one-dimensional slices through both the summed counts and model maps (the area covered by these slices is indicated by the boxes drawn on the stacked maps; their width motivated in each case by the LAT PSF as described in §3, to match the regions within which upper limits are computed:  $1^\circ$ ,  $0.4^\circ$  and  $0.2^\circ$  for the  $\geq 300$  MeV,  $\geq 3$  GeV and  $\geq 30$  GeV datasets, respectively). Sources with a high individual TS ( $>16$ ), and those within  $0.2^\circ$  of a catalogue source are not included in the stack. The field containing the BCG A 3360 has also been removed, due to the proximity (within  $1^\circ$ ) of the very bright ( $(3.71 \pm 0.07) \times 10^{-8} \text{ph cm}^{-2} \text{s}^{-1}$ ) 2FGL source 2FGL J0538.8–4405. The model provides a reasonable description of the data, and there is no evidence for an excess close to the origin. Applying the method described in §3, the derived 95% upper limits on the  $\gamma$ -ray flux of an average source within the class of BCGs, given the cuts applied and within a region of size comparable with the LAT PSF, are found to be  $7.4 \times 10^{-11} \text{ph cm}^{-2} \text{s}^{-1}$  (within a  $1^\circ$  radius for  $300 \text{ MeV} \leq E \leq 300 \text{ GeV}$ ),  $7.1 \times 10^{-12} \text{ph cm}^{-2} \text{s}^{-1}$  (within a  $0.4^\circ$  radius for  $3 \text{ GeV} \leq E \leq 300 \text{ GeV}$ ) and  $3.7 \times 10^{-13} \text{ph cm}^{-2} \text{s}^{-1}$  (within a  $0.2^\circ$  radius for  $30 \text{ GeV} \leq E \leq 300 \text{ GeV}$ ).

#### 4.3 Sources of Note

##### 4.3.1 2FGL Sources

The *Fermi* source 2FGL J0627.1–3528 is associated with the BCG in A 3392, which is classified as a BL Lac object. It is listed with a 24-month detection significance of 12.6,  $100 \text{ MeV} \leq E \leq 100 \text{ GeV}$  flux of  $(1.50 \pm 0.18) \times 10^{-9} \text{ph cm}^{-2} \text{s}^{-1}$  and photon index of  $1.93 \pm 0.09$ . With 21 months more data (and in an energy band  $300 \text{ MeV} \leq E \leq 300 \text{ GeV}$ ) we calculate an increased detection significance of 14.9, and a consistent (within errors) photon index, as expected.

The *Fermi* source 2FGL J1958.4–3012 is associated with the BL Lac object RXC J1958.2–3011, and may be a BCG (see § 2). It is listed with a 24-month detection significance of 5.1,  $100 \text{ MeV} \leq E \leq 100 \text{ GeV}$  flux of  $(5.94 \pm 1.78) \times 10^{-10} \text{ph cm}^{-2} \text{s}^{-1}$  and photon index of  $1.9 \pm 0.2$ . With 21 months more data (and in an energy band  $300 \text{ MeV} \leq E \leq 300 \text{ GeV}$ ) we calculate an increased detection significance of 6.8, and a consistent (within errors) photon index, as expected.

##### 4.3.2 Offset Detections: Possible Counterparts

TS maps were constructed for candidate sources with  $\text{TS} \gtrsim 16$ , to better localise the source position. These can be seen in Figure 4 for the BCGs in MACS J1347.5–1145 ( $\text{TS} = 43.4$ ), RXC J0132.6–0804 ( $\text{TS} = 24.0$ ) and IC 4991 ( $\text{TS} = 16.0$ ), and illustrate the effect of neglecting to add the candidate to the model: significant sources are revealed and localised where the baseline model (containing all local 2FGL sources, and the diffuse Galactic and extragalactic backgrounds, see §3) fails to describe the  $\gamma$ -ray emission.

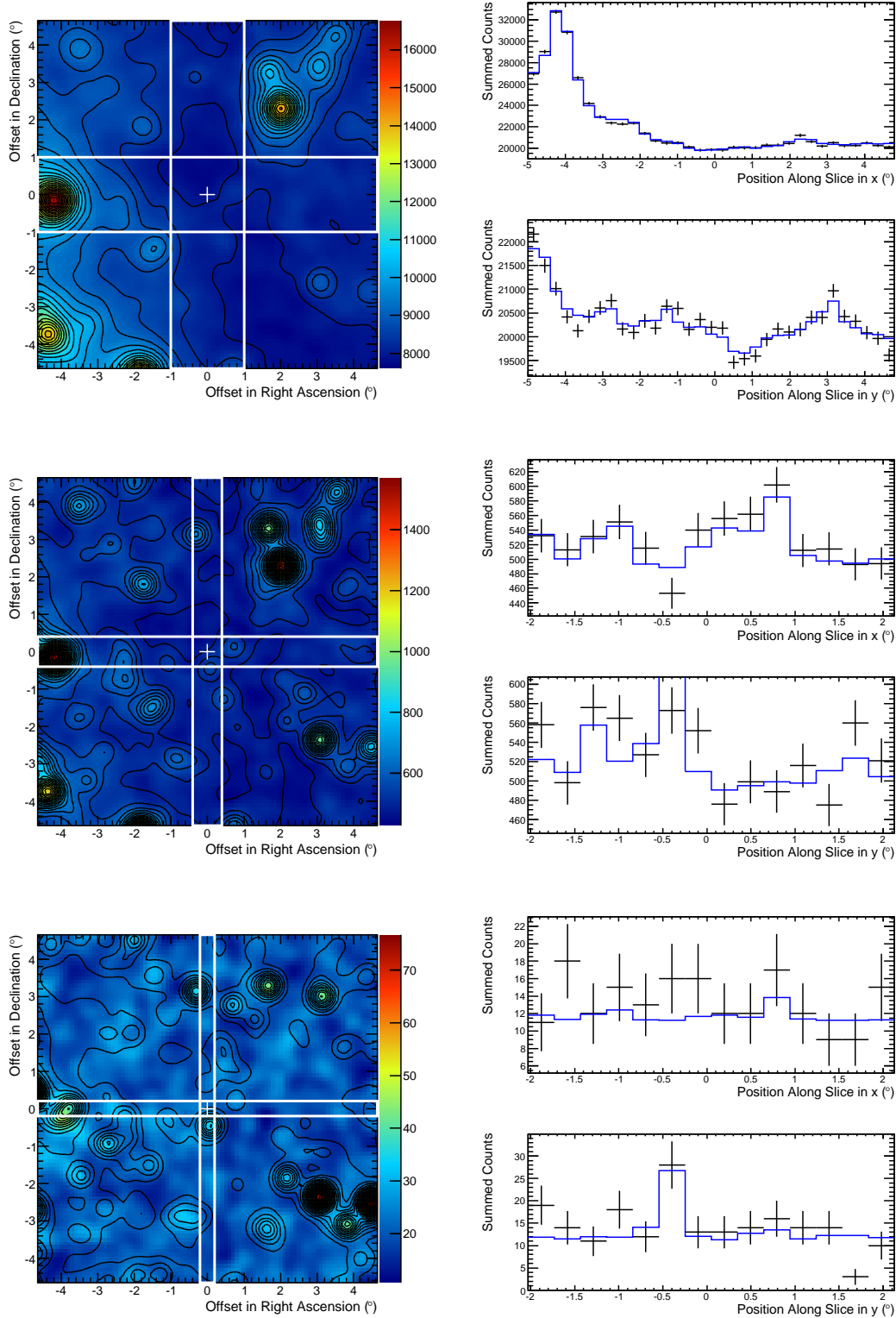


**Figure 3.** Stacked counts maps for the main sample of BCGs above an energy (**top**) 300 MeV, (**middle**) 3 GeV and (**bottom**) 30 GeV, overlaid with contours representing the corresponding stacked model maps (for the null hypothesis). The white cross indicates the BCG position in all fields. The stacked maps have been smoothed with a Gaussian kernel of rms  $0.2^\circ$ . A cut in candidate source TS above 16 has been applied, and additionally a *proximity* cut of  $0.2^\circ$  (to remove fields where the candidate position is coincident with a *Fermi*-LAT source). Neglecting also fields for which a 2FGL source brighter than  $1 \times 10^{-8}$  ph cm $^{-2}$ s $^{-1}$  is found to be within  $1^\circ$  of the central position (see §4.2), these stacks then comprise 109 (**top**) and 111 (**middle; bottom**) individual fields. The boxed regions indicate the area of the slices (to the right of each stack) through both maps in the horizontal and vertical directions, allowing a 1-D comparison between the data (black points) and null model (blue line).

These peaks in TS were fitted with parabolic ellipsoids and the best-fit peak positions are illustrated in the figure. The contours represent the 95% confidence regions for the positions of the sources.

Adding a candidate at the position of the BCG in MACSJ1347.5–1145 (in the energy band  $300 \text{ MeV} \leq E \leq 300 \text{ GeV}$ ) yields a photon index of  $2.76 \pm 0.01$  and a flux of  $(3.81 \pm 0.70) \times 10^{-9} \text{ ph cm}^{-2} \text{ s}^{-1}$ . The significant source in the field however, is clearly offset from the BCG position (the fitted peak in TS is located at Right Ascension (RA) =  $207.33^\circ$ , Declination (Dec.) =  $-11.55^\circ$ ) and so unlikely to be associated. Consulting the literature reveals the *Fermi*-LAT detection of a GeV flare consistent (within the quoted statistical errors) with this location in November 2011 (ATel #3788), and the flat-spectrum  $z = 0.34$  Quasi Stellar Object (QSO) PKS 1346–112 (Jackson et al. 2002), is given as a possible counterpart. Following this detection, a possible Wide-field Infrared Survey Explorer (WISE) blazar counterpart was identified, coincident with the radio source (ATel #4086). Re-running the likelihood analysis with this new source included in the model yields a negligible TS at the BCG position, and a TS of 179.6 (corresponding to a detection significance of  $\approx 13.4\sigma$ ) at the peak position, with a corresponding photon index of  $2.44 \pm 0.03$  and flux of  $(3.04 \pm 0.15) \times 10^{-8} \text{ ph cm}^{-2} \text{ s}^{-1}$ . Despite the high TS value, the transient nature of the source may account for its absence from the 2FGL.

Adding a candidate at the position of the BCG in RXCJ0132.6–0804 (in the energy band  $300 \text{ MeV} \leq E \leq 300 \text{ GeV}$ ) yields for the source a photon index of  $2.20 \pm 0.02$  and a flux of  $(1.42 \pm 0.50) \times 10^{-9} \text{ ph cm}^{-2} \text{ s}^{-1}$ . There appear to be two significant sources in the field, the more central of which (the fitted TS peak is located at RA =  $23.25^\circ$ , Dec. =  $-7.98^\circ$ ), is  $8'$  from the BCG and may be associated with a member of the parent cluster. The most significant peak is fitted to a position at RA =  $21.78^\circ$ , Dec. =  $-8.37^\circ$ . The BL Lac FBQS J0127–0821 at a redshift of 0.36 is a plausible  $\gamma$ -ray counterpart (Plotkin et al. 2008). A re-analysis of the field using a model containing these two localised sources nullifies the BCG TS, and results in a TS of 28.0 for the closer peak, and 65.0 for the remaining one, corresponding to  $\approx 5.3\sigma$  and  $\approx 8\sigma$  detections, respectively. A photon index of  $2.36 \pm 0.03$  and flux of  $(1.14 \pm 0.06) \times 10^{-8} \text{ ph cm}^{-2} \text{ s}^{-1}$  is calculated for the latter, and for the former a photon index of  $1.98 \pm 0.03$ , and a flux of  $(3.06 \pm 0.24) \times 10^{-9} \text{ ph cm}^{-2} \text{ s}^{-1}$ .

Adding a candidate at the position of the BCG in IC 4991 (in the energy band  $300 \text{ MeV} \leq E \leq 300 \text{ GeV}$ ) yields a photon index of  $2.379 \pm 0.009$  and a flux of  $(1.64 \pm 0.62) \times 10^{-9} \text{ ph cm}^{-2} \text{ s}^{-1}$ . There appear to be two potential non-2FGL sources of  $\gamma$  radiation in the field. For the first, the BCG lies just outside the 95% confidence contour (the fitted peak in TS is located at RA =  $304.30^\circ$ , Dec. =  $-41.22^\circ$ ). If this TS peak represents a genuine  $\gamma$ -ray source, it may be associated with the candidate, or perhaps with the ROSAT source 1RXS 201731.2–411452, a BL Lac object  $6'$  removed (Kollatschny et al. 2008). The second TS peak (fit position: RA =  $307.27^\circ$ , Dec. =  $-42.72^\circ$ ) may indicate  $\gamma$ -ray emission associated with an 81 mJy SUMSS source  $5'$  removed, that is not clearly identified (see Mauch et al. (2003)). Remodelling the data to account for these two sources renders the candidate BCG emission insignificant (reducing the TS to 2.7), and results in a TS of 13.9 for the

**Table 2.** A summary of non-2FGL *Fermi* detections of sources in fields within our sample, giving the fitted position (and error) of the TS peak, and the output TS after remodelling the data. No attempt is made to account for trials factors due to the large sample considered, but we note that a TS value of  $>25$  still corresponds to a post-trials significance of  $>4\sigma$ .

Name	TS*	RA <sup>†</sup> (°)	Dec <sup>‡</sup> (°)	Error (°)
FERMI J1350–1140 <sup>††</sup>	179.8	207.33	–11.55	0.11
FGL J0133.0–0758	28.2	23.25	–7.98	0.16
FGL J0127.1–0822	64.8	21.78	–8.37	0.14
FGL J2029.0–4243	41.3	307.27	–42.72	0.22

\* Test Statistic

† Right Ascension

‡ Declination

†† Detected by the Fermi Large Area Telescope Collaboration in November 2011 (ATel #3788)

closer peak, and 41.1 for the peak revealed toward the edge of the field, roughly corresponding to statistical significances of  $3.7\sigma$  and  $6.4\sigma$ , respectively. A photon index of  $2.2 \pm 0.2$  and flux of  $(8.58 \pm 3.15) \times 10^{-9} \text{ ph cm}^{-2} \text{ s}^{-1}$  is calculated for the significant source.

Table 2 summarises the detections confirmed after a remodelling to account for sources of  $\gamma$ -ray emission in the three fields described above was carried out. The TS maps were re-calculated based on the new output models, which were found to describe the emission adequately.

#### 4.3.3 $\gamma$ -ray Emission from A 2055?

Using the  $3 \text{ GeV} \leq E \leq 300 \text{ GeV}$  data, analysis of the BCG in A 2055 (which is classified as a BL Lac object) results in a TS of 15.2. The corresponding TS map is shown in Figure 5. A hint of emission from the position of the BCG can be clearly seen. The position of the BCG is contained within the 95% confidence region for the source location. With this candidate alone added, the model sufficiently describes the  $\gamma$ -ray emission within the field. The source is not detected in the energy band  $30 \text{ GeV} \leq E \leq 300 \text{ GeV}$ , and the TS drops to 8.0 using the larger  $300 \text{ MeV} \leq E \leq 300 \text{ GeV}$  dataset.

## 5 DISCUSSION

There is no statistically significant evidence for emission within the stacked sample. The upper limits derived on an average source within the class of BCGs represent at least an order of magnitude improvement on the individual upper limits presented in Table 1. The derived limits are consistent with the expectation of a  $\sim 1/\sqrt{N_{\text{obj}}}$  scaling for the background-limited lower energy bands and  $\sim 1/N_{\text{obj}}$  for highest energies where the *Fermi*-LAT becomes signal limited even in the stacked sample, where  $N_{\text{obj}}$  is the number of fields stacked.

To derive a limit on the  $\gamma$ -ray to radio flux ratio ( $F_{1\text{GeV}}/F_{1.4\text{GHz}}$ ) for the core emission of the sample we consider the *core* radio flux (some fraction of the emission given in Table 1) of each BCG (Hogan et al. prep), and find an average radio flux of  $2.37 \times 10^{-15} \text{ erg cm}^{-2} \text{ s}^{-1}$  and an average luminosity of  $1.8 \times 10^{41} \text{ erg s}^{-1}$  (at an average redshift of

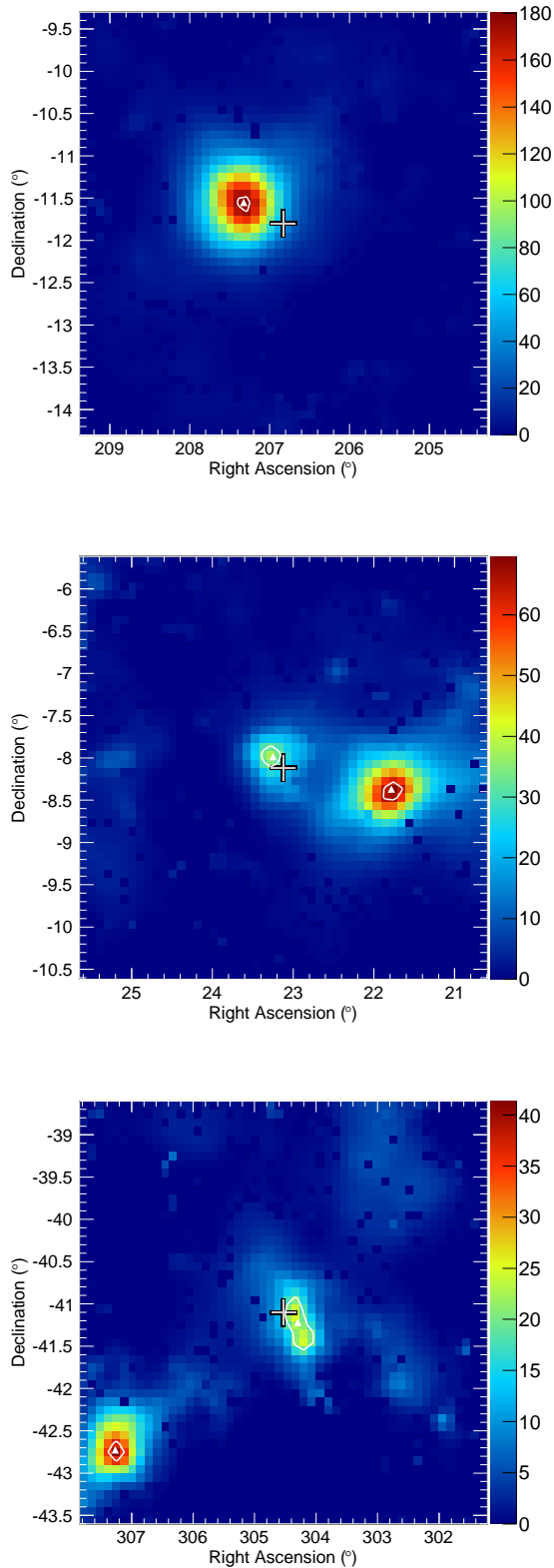


**Figure 4.** TS map for candidate sources in MACS J1347.5–1145 (**top**), RXC J0132.6–0804 (**middle**), and IC 4991 (**bottom**) produced from  $300 \text{ MeV} \leq E \leq 300 \text{ GeV}$  data. The BCG position is indicated by the central black/grey cross. Peaks in TS have been fitted with parabolic ellipsoids, the fit position for which is shown by a white triangle and given in table 2. The 95% confidence contours on source locations are shown in white.

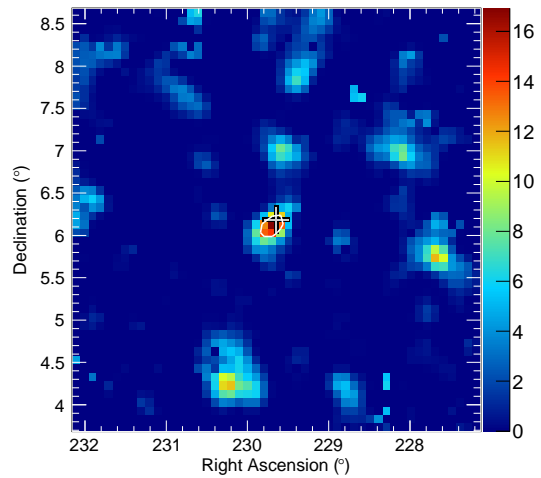


**Figure 5.** TS map for the candidate source in A 2055, produced from  $3 \text{ GeV} \leq E \leq 300 \text{ GeV}$  data. The BCG position is indicated by the central black/grey cross. The 95% confidence contour on the  $\gamma$ -ray source position is shown in white.

0.13). Given the upper limit on the stacked emission, the average  $\gamma$ -ray flux evaluated at 1 GeV and assuming a photon index of 2, is less than  $3.55 \times 10^{-14} \text{ erg cm}^{-2} \text{ s}^{-1}$ , and the average  $\gamma$ -ray luminosity is less than  $1.35 \times 10^{42} \text{ erg s}^{-1}$ . The average  $F_{1\text{GeV}}/F_{1.4\text{GHz}}$  of the sample is therefore  $<15$ . The  $\gamma$ -ray flux-limit for the sample corresponds to only 0.1% of the flux of NGC 1275, which has  $F_{1\text{GeV}}/F_{1.4\text{GHz}} \approx 120$  ( $\sim 90$  excluding  $\gamma$ -ray flares). The average core radio flux is  $\approx 1\%$  of that of NGC 1275. The lack of a  $\gamma$ -ray signal in the stack therefore implies that the average core-radio selected BCGs have spectral energy distributions with a different shape to that of NGC 1275, with significantly lower  $\gamma$ -ray flux relative to core radio flux, though the current highly variable state of  $\gamma$ -ray emission in this active galaxy (Kataoka et al. 2010) may account for the difference in  $F_{1\text{GeV}}/F_{1.4\text{GHz}}$ .

NGC 1275 and M 87 are the closest cooling-core BCGs, so the detected  $\gamma$ -ray emission is unlikely to be beamed toward us if they are drawn from a random distribution of sight lines. However, a role for beaming in NGC 1275 cannot be excluded and may play a role in its unusual  $\gamma$ -ray brightness (see above). It has been postulated (see Falceto-Gonçalves et al. (2010)) that the central AGN comprises a viscous accretion disk tilted with respect to the rotating super-massive black hole, bringing about precessing jets as a result of torques acting on the disk. Very Long Baseline Interferometry (VLBI) maps of the radio source can place constraints on the inclination of the system: to be satisfied, some curvature of the jet away from the line of sight is implied (Dunn et al. 2006). This said, for those BCGs with bona fide BL Lac nuclei, for example A 2055 and A 3392, which are significantly more distant and comparable to most of the parent sample, the probability of observing a few sources close to the jet direction is significant.

We can assess the number of local clusters hosting a *Fermi*-LAT AGN by cross-correlating the Abell cluster catalogue of 5250 clusters (including the supplementary systems) (Abell et al. 1989), with the 2FGL. Of the 85 coincidences within  $20'$ , only 11 are consistent with the 2FGL

source being a cluster member and of those only four being the BCG (NGC 1275 in A 426/Perseus, PKS 0625–35 in A 3392, PKS 2035–714 in A 3701 and PKS 2316–423 in S1111). The latter two clusters are not detected above the X-ray flux limit for the eBCS or REFLEX catalogues, so were not considered in the analysis above. Therefore, the chance of finding a *Fermi* source in any particular cluster is relatively small but is significant.

The added complication with the analysis is that the *Fermi*-LAT spatial resolution and source density ( $\approx 0.05$  per square degree) implies chance coincidences on the order of a few when more than 100 positions are considered. This is illustrated in Figure 4, given that the TS output from the initial binned likelihood analysis of the field was in each case not exclusively associated with the BCG under scrutiny, but a nearby source of emission not described by the model. The angular resolution of the *Fermi*-LAT is sufficient (particularly above 1 GeV) to isolate nearby background sources from the position of interest in most cases, but the likelihood analysis is not robust enough to accurately disentangle the  $\gamma$  emissions in such an event.

Four *detections* (that is, of  $TS > 25$  emission) have been made of sources not contained in the 2FGL (see Table 2). For those above a TS of  $\sim 50$ , their absence from the 2FGL implies temporal variability in the emission, as appears to be the case for the source FERMI J1350–1140. A more detailed study of these sources is left to future work. The tentative evidence for emission from the BCG in A 2055 will be refuted or validated in time: if the significance of emission from the source position continues to increase, it will be the fourth such source to be detected using *Fermi*; the second BCG hosting a BL Lac.

## 6 CONCLUDING REMARKS

The *Fermi*-LAT detection of a few sources in clusters of galaxies sets important limits on the energetics and emission mechanisms at work in the cores of the most massive member galaxies. The detections of BCGs using *Fermi* are strongly biased toward the most radio bright systems or those that are dominated by a beamed core. Our statistical upper limit from a larger sample of sources with lower radio flux indicates that the average core-radio selected BCG is more than an order of magnitude less  $\gamma$ -ray luminous than, for example, NGC 1275. Furthermore the ratio of  $\gamma$ -ray to radio flux is  $< 15$ , compared with  $F_{1\text{GeV}}/F_{1.4\text{GHz}} \approx 120$  for NGC 1275. The BCG in A 2055, which hosts a BL Lac, may soon be detectable in HE  $\gamma$  rays (given a longer exposure using *Fermi*), and if so, will corroborate this conclusion.

Detections of a number of new sources are declared; though none of these appear to be unambiguously associated with the BCG, the slightly-offset emission in the field of RXC J0132.6–0804 might be associated with the candidate, or else another cluster member galaxy, and in the field of IC 4991 may (if genuine) in part originate from the BCG. This work also illustrates then, the need to carefully assess all the possible sources of emission that could explain the *Fermi*-LAT detections found in clusters before attributing them to (for example) cluster merger-related shocks or DM annihilation.

## ACKNOWLEDGMENTS

The authors would like to thank Stefan Ohm for useful comments and discussions. This work has made use of public *Fermi* data and Science Tools provided by the *Fermi* Science Support Centre. K. L. Dutson and R. J. White acknowledge support from the STFC and J. A. Hinton from the Leverhulme Trust.

## REFERENCES

- Abdo A. A., et al., 2009a, *ApJ*, 699, 31  
 Abdo A. A., et al., 2009b, *Phys. Rev. D*, 80, 122004  
 Abell G. O., Corwin Jr. H. G., Olowin R. P., 1989, *ApJS*, 70, 1  
 Abramowski A., et al., 2012, *ApJ*, 746, 151  
 Ackermann M., et al., 2010a, *J. Cosmol. Astropart. Phys.*, 5, 25  
 Ackermann M., et al., 2010b, *ApJ*, 717, L71  
 Aharonian F., et al., 2006, *Science*, 314, 1424  
 Aharonian F. A., 2002, *MNRAS*, 332, 215  
 Aleksić J., et al., 2012, *A&A*, 539, L2  
 Antonucci R., 1993, *Annu. Rev. Astron. Astrophys.*, 31, 473  
 Asada K., Kameno S., Shen Z.-Q., Horiuchi S., Gabuzda D. C., Inoue M., 2006, *PASJ*, 58, 261  
 Atwood W. B., et al., 2009, *ApJ*, 697, 1071  
 Benson A. J., Bower R. G., Frenk C. S., Lacey C. G., Baugh C. M., Cole S., 2003, *ApJ*, 599, 38  
 Biretta J. A., Stern C. P., Harris D. E., 1991, *ApJ*, 101, 1632  
 Blasi P., Colafrancesco S., 1999, *Nucl. Phys. B Proceedings Supplements*, 70, 495  
 Blasi P., Gabici S., Brunetti G., 2008, *IJMPA*, 22, 681  
 Böhringer H., Schuecker P., Guzzo L., Collins C. A., Voges W., Cruddace R. G., Ortiz-Gil A., Chincarini G., De Grandi S., Edge A. C., MacGillivray H. T., Neumann D. M., Schindler S., Shaver P., 2004, *A&A*, 425, 367  
 Bower R. G., Benson A. J., Malbon R., Helly J. C., Frenk C. S., Baugh C. M., Cole S., Lacey C. G., 2006, *MNRAS*, 370, 645  
 Brown M., Adams J., 2011, *MNRAS*, 000, 1  
 Burns J. O., 1990, *AJ*, 99, 14  
 Cavagnolo K. W., Donahue M., Voit G. M., Sun M., 2008, *ApJ*, 683, L107  
 Clarke T. E., Sarazin C. L., Blanton E. L., Neumann D. M., Kassim N. E., 2005, *ApJ*, 625, 748  
 Condon J. J., Cotton W. D., Greisen E. W., Yin Q. F., Perley R. A., Taylor G. B., Broderick J. J., 1998, *AJ*, 115, 1693  
 Dunn R. J. H., Fabian A. C., Sanders J. S., 2006, *MNRAS*, 366, 758  
 Ebeling H., Edge A. C., Allen S. W., Crawford C. S., Fabian A. C., Huchra J. P., 2000, *MNRAS*, 000, 000  
 Ebeling H., Edge A. C., Böhringer H., Allen S. W., Crawford C. S., Fabian A. C., Voges W., Huchra J. P., 1998, *MNRAS*, 301, 881  
 Ebeling H., Edge A. C., Henry J. P., 2001, *ApJ*, 553, 668  
 Edge A. C., Stewart G. C., Fabian A. C., Arnaud K. A., 1990, *MNRAS*, 245, 559  
 Fabian A. C., 1994, *Annu. Rev. Astron. Astrophys.*, 32, 277

- Fabian A. C., Allen S. W., Crawford C. S., Johnstone R. M., Morris R. G., Sanders J. S., Schmidt R. W., 2002, *MNRAS*, 332, L50
- Fabian A. C., Sanders J. S., Etori S., Taylor G. B., Allen S. W., Crawford C. S., Iwasawa K., Johnstone R. M., Ogle P. M., 2000, *MNRAS*, 318, L65
- Falceto-Gonçalves D., de Gouveia Dal Pino E. M., Gallagher J. S., Lazarian A., 2010, *ApJ*, 708, L57
- Hinton J. A., Domainko W., Pope E. C. D., 2007, *MNRAS*, 382, 466
- Hlavacek-Larrondo J., Fabian A. C., Sanders J. S., Taylor G. B., 2011, *MNRAS*, 415, 3520
- Hogan M. T., et al., in prep
- Huber B., Farnier C., Manalaysay A., Straumann U., Walter R., 2012, *ArXiv e-prints*
- Jackson C. A., Wall J. V., Shaver P. A., Kellermann K. I., Hook I. M., Hawkins M. R. S., 2002, *A&A*, 386, 97
- Kataoka J., et al., 2010, *ApJ*, 715, 554
- Kollatschny W., Kotulla R., Pietsch W., Bischoff K., Zetzl M., 2008, *A&A*, 484, 897
- Mattox J. R., et al., 1996, *ApJ*, 461, 396
- Mauch T., Murphy T., Buttery H. J., Curran J., Hunstead R. W., Piestrzynski B., Robertson J. G., Sadler E. M., 2003, *MNRAS*, 342, 1117
- McNamara B. R., Nulsen P. E. J., 2007, *Annu. Rev. Astron. Astrophys.*, 45, 117
- McNamara B. R., Wise M., Nulsen P. E. J., David L. P., Sarazin C. L., Bautz M., Markevitch M., Vikhlinin A., Forman W. R., Jones C., Harris D. E., 2000, *ApJ*, 534, L135
- Mittal R., Hudson D. S., Reiprich T. H., Clarke T., 2009, *A&A*, 501, 835
- Nolan P. L., et al., 2012, *ApJS*, 199, 31
- Paggi A., Massaro F., D’Abrusco R., 2012, *The Astronomer’s Telegram*, 4086, 1
- Peterson J. R., Kahn S. M., Paerels F. B. S., Kaastra J. S., Tamura T., Bleeker J. A. M., Ferrigno C., Jernigan J. G., 2003, *ApJ*, 590, 207
- Pfrommer C., Enßlin T. A., 2004, *A&A*, 413, 17
- Plotkin R. M., Anderson S. F., Hall P. B., Margon B., Voges W., Schneider D. P., Stinson G., York D. G., 2008, *ApJ*, 135, 2453
- Rolke W. A., López A. M., Conrad J., 2005, *Nuclear Instruments and Methods in Physics Research A*, 551, 493
- Russell H. R., Fabian A. C., Sanders J. S., Johnstone R. M., Blundell K. M., Brandt W. N., Crawford C. S., 2010, *MNRAS*, 402, 1561
- Sijacki D., Springel V., Di Matteo T., Hernquist L., 2007, *MNRAS*, 380, 877
- Sparks W. B., Biretta J. A., Macchetto F., 1996, *ApJ*, 473, 254
- Torresi E., D’Ammando F., 2011, *The Astronomer’s Telegram*, 3788, 1
- Vermeulen R. C., Readhead A. C. S., Backer D. C., 1994, *ApJ*, 430, 41
- Völk H. J., Atoyan A. M., 1999, *Astropart. Phys.*, 11, 73
- Wise M. W., McNamara B. R., Nulsen P. E. J., Houck J. C., David L. P., 2007, *ApJ*, 659, 1153